

25. CHEMICAL COMPOSITION OF IGNEOUS ROCKS AND ORIGIN OF THE SILL AND PILLOW-BASALT COMPLEX OF NAURU BASIN, SOUTHWEST PACIFIC¹

Hidekazu Tokuyama, Ocean Research Institute, University of Tokyo, Nakano, Tokyo 164, Japan
and

Rodey Batiza, Department of Earth and Planetary Sciences, Washington University, St. Louis, Missouri

ABSTRACT

The sill and pillow complex cored on Deep Sea Drilling Project Leg 61 (Site 462) is divided into two groups, A and B types, on the basis of chemical composition and volcanostratigraphy. The A-type basalt is characterized by a higher FeO^*/MgO ratio and abundant TiO_2 , whereas the B-type basalt is characterized by a lower FeO^*/MgO ratio and scarcity of TiO_2 . The A type is composed of sills interbedded with hyaloclastic sediments, and the B type consists of basalt sills and pillow basalt with minor amounts of sediment. However, the structure of pillow basalts in the B type is atypical; they might be eruptive. From paleontological study of the interbedded sediments and radiometric age determination of the basalt, the volcanic event of A type is assumed to be Cenomanian to Aptian, and that of B type somewhat older. The oceanic crust in the Nauru Basin was assumed to be Oxfordian, based on the Mesozoic magnetic anomaly. Consequently, two events of intraplate volcanism are recognized. It is thus assumed that the sill-pillow complex did not come from a normal oceanic ridge, and that normal oceanic basement could therefore underlie the complex.

The Site 462 basalts are quartz-normative, and strongly hypersthene-normative, and have a higher FeO^*/MgO ratio and lower TiO_2 content. Olivine from the Nauru Basin basalts has a lower $\text{Mg}/(\text{Mg} + \text{Fe}^{2+})$ ratio (0.83–0.84) and coexists with spinel of lower $\text{Mg}/(\text{Mg} + \text{Fe}^{2+})$ ratio when compared to olivine-spinel pairs from mid-ocean ridge (MAR) basalt. The glass of spinel-bearing basalts has a higher $\text{FeO}^*/(\text{FeO}^* + \text{MgO})$ ratio (0.58–0.60) than that of MAR (<0.575). Therefore, the Nauru Basin basalts are chemically and mineralogically distinct from ocean-ridge tholeiite. That the Nauru Basin basalts are quartz-normative and strongly hypersthene-normative and have a lower TiO_2 content suggests that the basaltic liquids of Site 462 were generated at shallower depths (<5 kbar) than ocean-ridge tholeiite: Site 462 basalts are similar to basalts from the Manihiki Plateau and the Ontong-Java Plateau, but different from Hawaiian tholeiite of hot-spot type, with lower K_2O and TiO_2 content. We propose a new type of basalt, ocean-plateau tholeiite, a product of intraplate volcanism.

INTRODUCTION

Holes 462 and 462A, drilled on DSDP Leg 61, penetrated about 560 meters of turbiditic and volcanic sediments before a sill-pillow complex was reached. Total penetration of Holes 462 and 462A was 617 and 1068.5 meters, respectively. Both holes were abandoned before reaching ocean-ridge tholeiite formed at the normal oceanic ridge. The petrology of these volcanoclastic silts and sands is described in other sections of this volume. The oldest sediment interbedded with the sill-pillow complex is Barremian. The underlying oceanic crust at Site 462 in the Nauru Basin was assumed to be 148 m.y. old (Oxfordian), based on the Mesozoic magnetic anomaly (Cande et al., 1978). The lithological sequence of the sill-pillow complex is quite different from that formed at oceanic ridges. Also, chemical compositions of this complex are slightly different from ocean-ridge tholeiite. The main body of this report deals with the geological setting, chemical composition, mineralogy, and petrology of the sill-pillow complex cored at Site 462, in the Nauru Basin.

GEOLOGICAL SETTING

Site 462 is located at $7^\circ 14.50' \text{N}$, $165^\circ 01.90' \text{E}$, in the Nauru Basin. Drilling here penetrated a mid-Cretaceous

volcanic complex more than 500 meters thick that presumably overlies a volcanic basement of Late Jurassic age (M-26). This complex represents a voluminous, non-edifice-building, off-ridge outpouring of magma, chemically different from mid-oceanic ridge tholeiite.

Three acoustic layers can be identified, based on the seismic records in the vicinity of Site 462 (Voyages of *Kana Keoki*, 1977; *Hakurei Maru*, 1977; and *Glomar Challenger*, 1978). The first layer, with a thickness of 0.46 sec two-way reflection time, is characterized by many higher-frequency sets of stratified reflectors. However, they become transparent near the bottom of this layer. The layer proved to be Cenozoic turbidite deposits. The second layer, with a thickness of 0.15 sec two-way reflection time, is characterized by slightly higher-frequency sets of stratified reflectors. The top of the layer correlates with chert beds in the middle Eocene. The main part of this layer consists of Late Cretaceous turbidite deposits. The third layer is characterized by low-frequency sets of smooth reflectors. The layer consists of a sill-pillow complex, interbedded with sediment. The lower boundary of the layer is unclear, but the thickness of the layer may have more than a 0.4-sec two-way reflection time, and an estimated thickness of more than 700 meters. The layer cannot be correlated with Oceanic Layer 2, because the volcanic rocks from the layer are significantly different from ocean-ridge tholeiite, and these volcanics are mainly intrusive into

¹ Initial Reports of the Deep Sea Drilling Project, Volume 61.

sediments. Therefore, normal oceanic basement underlies the third layer as deduced from the magnetic survey. The seafloor in the Nauru Basin is 1 km shallower than predicted for a cooling slab of this age (Sclater and Francheteau, 1970). The anomalous shallower depth of the Nauru Basin might be caused by the thicker third layer. The low-frequency reflectors are assumed to be widespread over the Nauru Basin, with a maximum diameter and average thickness more than 500 km and 500 m, respectively. Although the dimensions of this distribution are smaller than those of the anomalously shallow Caribbean sea floor (Burke et al., 1978), the Nauru Basin is a kind of anomalously shallow ocean floor, in view either of the acoustic nature (Talwani et al., 1977) and the thick pile of the sill-pillow complex interbedded with sediment (Worzel, Bryant, et al., 1973) in the Caribbean. On the other hand, the estimated total volume of the volcanics from the Nauru Basin is almost identical to that of plateau basalt (Deccan Plateau area 500,000 km², maximum thickness 2 km; Subramanian and Sahasrabudhe, 1964) and concordant injection (Karoo dolerite distribution area 572,000 km², average thickness 600–1000 m; Walker and Poldervaart, 1949).

STRATIGRAPHY AND LITHOLOGY OF THE SILL-PILLOW COMPLEX

Hole 462A reached basalt flow, in Core 14, Section 2 at a depth of 564 meters below the volcanic sediment. A further 504.5 meters of section which consists of about 58 meters (11.5%) of hyaloclastic sediments, 110 meters (21.8%) of pillow basalts, and 336.5 meters (66.7%) of basalt sills, has been drilled. Recovery of sediment and the sill-pillow complex averaged about 56%. Thirty-eight intrusives and six extrusives were tentatively identified, based on differences in any one or a combination of physical, textural, or lithologic attributes (see Site Summary, this volume).

The intrusive unit is divided into two groups: single basalt sills and multiple basalt sills. The single sills have been recognized by the following characteristics: (1) glassy margins or fine-grained marginal zone with sub-horizontal attitude, and (2) orderly, inward-coarsening grain-size variation, coarse-grained interiors, and diabasic texture. The single basalt sills were easily recognized and usually distinguished as individual units. Units 6, 12, 13, 21, and 25 (see Site Summary, this volume) are examples of single basalt sills. Their thickness ranges from a few tens of centimeters to over 50 meters. In some cores, contacts between baked sediment and glass were recovered, but usually the glassy sill margins were not recovered. In the latter case, however, narrow, fine-grained marginal zones were recognized. The sill units exhibit a narrow range of mineralogic and chemical variation, and the thicker ones (5–10 m) invariably contain granophyric schlieren.

A multiple sill is more difficult to distinguish with certainty. In some cases (e.g., Units 33 and 34), where fine-grained to glassy apophyses are present, multiple intrusion, at least on a small scale, can be demonstrated.

On the larger scales, it has been inferred by the presence of alternating fine-grained and coarser-grained units (as in Units 31 and 33), without glassy margins of which recovery was very high in drill core. In such cores, abrupt changes in grain size across horizontal or near-horizontal contacts are observed. These observations support the interpretation that the units represent multiple intruded sills.

The mode of multiple intrusion from upper parts of sills (e.g., Units 1–5) is characterized by subtle grain size variations, but distinct mineralogical differences between individual units. This type of multiple intrusion may represent sequential emplacements of one magma batch in a series of several smaller batches, whereas the mode of multiple intrusion from the lower part of the complex is characterized by greater differences in grain size and absence of mineralogical differences between the various grain-size domains. Units of this type are associated with units of obvious extrusive character, especially in portions of a thick flow. In some cases, multiple intrusive units of the second type have been included in the unit with basalt flows (e.g., Unit 22), but in other cases they have been distinguished as separate units (e.g., Unit 27). This difference is based on the degree of abruptness in the transition between extrusive and multiple intrusive rocks, so that it is somewhat arbitrary. It reflects our judgment that the multiple intrusive is either a part of a thick flow or a true multiple-intrusive unit.

Pillow basalts show the following characteristics: (1) variable but small thickness (0.3–2 m) of units, (2) thick (up to 4 cm), glassy margins with variable attitudes (dips range from horizontal to vertical), (3) fine-grained throughout, but rarely coarse grained, (4) cooling cracks normal to ubiquitous glassy surfaces, and numerous un-oriented cracks in the interior. These characters suggest strongly that these units (e.g., 23, 26, 29, and 34) could have been extruded into sea water or intruded into unconsolidated water-rich sediments just under the sea floor, but they lack some of the characteristics of pillow lava, that is, radial cooling fractures, interpillowed paragonite, regular curved surfaces, and concentric structures. The mode of extrusion of these flows is more like brecciated pillows rather than typical pillow lava.

The upper part of the complex from 564 to 730 meters in Hole 462A has intercalated sills and hyaloclastic sedimentary units, whereas the lower part of the complex, from 730 to 1068.5 meters, consists of basalt sills and pillow basalts, with minor amounts of sediment. The paleontological age of sediments interbedded with the lower part is probably Barremian, whereas the age of sediments interbedded with the upper part ranges in the wider interval from Cenomanian to Barremian. Pillow basalt was first recovered at the boundary between the upper and lower parts. The radiometric age of the upper part is 110 ± 3 m.y. (isochron age), and that of lower part is 131 ± 15 m.y. (total-fusion age; Ozima, this volume). Moreover, from the paleomagnetic data, the paleolatitudes of the hyaloclastic sediments of Ceno-

manian age are approximately 30°S and 18°S, respectively (Steiner, this volume). Consequently, there could be a significant time gap between volcanic events.

As discussed above, the sill-pillow complex from Site 462 is divided into 2 types:

Type A, 564 to 730 meters: Sill (intruded into hyaloclastic sediments).

Type B, 730 to 1068.5 meters: Sill and pillow complex (alternation of intrusions and extrusions), with minor amount of sediments.

The presence of hyaloclastites supports the suggestion that at least part of the major Nauru Basin volcanic episode was extrusive. Huge concordant injections on land, like the Palisade diabase and Karroo dolerite, also are associated with extrusive lavas of the same age.

BASALT CHEMISTRY

About 130 samples from Hole 462A were analyzed for Si, Al, Ti, Mg, Fe, Ca, and K, and about 15 for Mn and P, using shipboard X-ray-fluorescence (XRF) techniques (Jacques, this volume). In addition, eight samples were analyzed for Si, Ti, Al, Fe²⁺, Fe³⁺, Mn, Mg, Ca, Na, K, P, H₂O⁻, and H₂O⁺ by wet chemical analyses, and Ni, Cr, Co, and S by atomic-absorption spectrometry (Table 1). The rocks display a relatively narrow range of TiO₂, K₂O, MgO, CaO, and SiO₂ contents, but unusually large variation in the abundance of Al₂O₃ and FeO in the light of the narrow variation of the other major oxides. There are no significant chemical changes within individual sills, except the granophyre schlieren in thicker sills, so that differentiation which might be

caused by minor removal of phenocryst phases during the slow cooling is not apparent.

The chemical compositions of fresh basalts from Hole 462A are plotted in terms of the ratio FeO*/MgO versus TiO₂ (Fig. 1). On this figure, two types are identified on the basis of differences in TiO₂ content and the FeO*/MgO ratio: (1) higher FeO*/MgO and richer TiO₂, and (2) lower FeO*/MgO and poorer in TiO₂. The chemical composition of type A corresponds to the former, and that of type B to the latter. Fujii et al. (this volume) reported that the A-type basalt is enriched in the large cations (Ba and Rb) and high-valency cations (Ti and P) compared to those of the B-type basalt. The fact that the glassy chilled margins of the A type are characterized by microphenocrysts of clinopyroxene, and rare olivine, and that those of the B type are characterized by microphenocrysts of olivine and rare clinopyroxene, is reflected by the difference between the FeO*/MgO ratios of the two types.

This is apparently explained by differentiation in the magma reservoir. Mazzullo and Bence (1976) reported that if the FeO*/MgO ratio of a basalt reflects the degree of crystal fractionation of ferromagnesian phases out of primary magma, then a covariation diagram of the FeO*/MgO ratio versus TiO₂ (incompatible with fractionating olivine or plagioclase) may be used to compare relative degrees of low-pressure fractionation in abyssal tholeiites, providing clinopyroxene is not an important fractionating phase. If this differentiation is caused by olivine removal, the Ni content of A type must be significantly lower than that of B type. How-

Table 1. Chemical composition and CIPW norms of basalts from Site 462 (wet chemical analyses) (Analyst: H. Haramura).

Component	Hole 462A						Hole 462	
	17-2, 84-86 cm	20-1, 116-121 cm	50-3, 130-134 cm	65-1, 59-61 cm	72-3, 21-23 cm	74-4, 25-31 cm	64-1, 8-11 cm	66-1, 23-25 cm
SiO ₂ (%)	47.90	47.50	48.75	48.87	49.24	48.83	49.78	48.30
TiO ₂	1.39	1.62	0.91	0.99	1.02	1.15	1.52	1.55
Al ₂ O ₃	14.76	14.69	15.20	15.58	15.33	15.36	14.76	15.45
Fe ₂ O ₃	3.78	2.88	3.63	3.29	3.52	3.89	3.62	3.16
FeO	7.96	10.15	6.85	7.70	7.30	7.56	9.07	9.30
MnO	0.25	0.26	0.19	0.19	0.19	0.19	0.21	0.20
MgO	7.33	7.09	8.39	7.83	7.70	7.59	7.01	6.76
CaO	11.77	11.14	12.02	11.47	12.29	11.05	9.44	10.81
Na ₂ O	2.27	2.26	1.94	1.96	1.95	2.05	2.19	2.23
K ₂ O	0.05	0.05	0.04	0.03	0.05	0.63	0.12	0.10
P ₂ O ₅	0.15	0.18	0.12	0.11	0.13	0.12	0.17	0.18
H ₂ O(+)	1.09	0.82	1.00	1.00	0.99	1.15	1.08	1.02
H ₂ O(-)	1.12	1.08	0.79	0.77	0.81	0.85	0.67	0.65
Total	99.82	99.72	99.83	99.79	100.52	100.42	99.64	99.71
Ni (ppm)	85	86	103	91	91	77	77	84
Co	18	12	5	5	20	14	11	11
Cr	110	132	82	85	220	77	77	116
S	200	130	100	140	160	680	280	460
FeO*/MgO	1.550	1.797	1.206	1.360	1.359	1.457	1.759	1.796
Type	A	A	B	B	B	B	B	A
Q	0.33	0.0	1.24	1.71	1.99	0.71	4.60	1.10
Or	0.30	0.30	0.24	0.18	0.30	3.78	0.72	0.60
Ab	19.68	19.55	16.74	16.92	16.71	17.62	18.93	19.25
An	30.67	30.45	33.30	34.30	33.35	31.34	30.74	32.49
Ne	0.0	0.0	0.0	0.0	0.0	0.0	0.0	0.0
Wo	11.75	10.37	11.16	9.61	11.50	9.84	6.67	8.77
En	7.24	5.58	7.38	5.95	7.29	6.22	3.83	4.88
Fs	3.83	4.45	2.98	3.09	3.48	3.00	2.53	3.56
En	11.46	10.51	13.93	13.94	12.14	12.99	14.00	12.30
Fs	6.07	8.37	5.62	7.25	5.80	6.27	9.26	8.97
Fo	0.0	1.38	0.0	0.0	0.0	0.0	0.0	0.0
Fa	0.0	1.21	0.0	0.0	0.0	0.0	0.0	0.0
Mt	5.61	4.27	5.37	4.87	5.17	5.73	5.36	4.67
Il	2.70	3.15	1.76	1.92	1.96	2.22	2.95	3.00
Ap	0.36	0.43	0.28	0.26	0.31	0.28	0.40	0.43

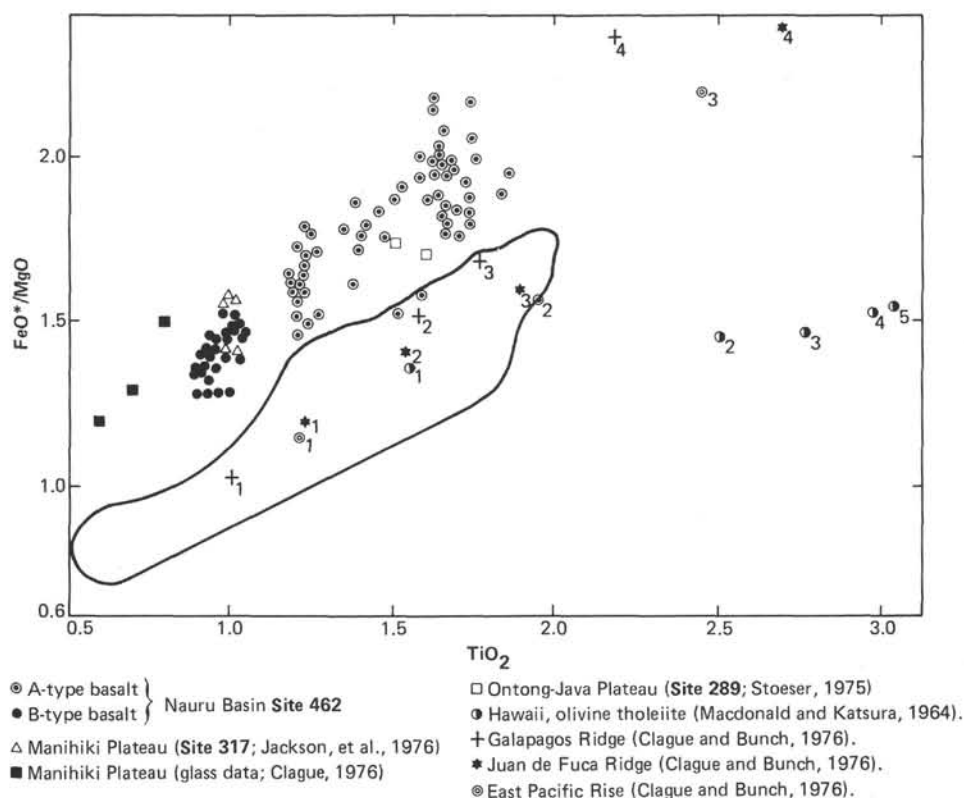


Figure 1. Covariation of FeO^*/MgO and TiO_2 . Numbers indicate the differentiation trend.

ever, these are no large differences, in Ni content between the two types (Table 1), so that this difference is explained by approximately 2% removal of olivine (Fo_{84} ; Ni 1100 ppm) from type B. In this model, we can never explain the variation of FeO^*/MgO ratios between the two types. Therefore, it seems unreasonable that the difference is caused by differentiation, and rather that the original magma of A type is different from that of B type.

In comparison with the FAMOUS glass data (Bryan et al., 1976) and bulk composition and fractionation trends of the Galapagos Ridge and the East Pacific Rise (Clague and Bunch, 1976), Hole 462A material is characterized by a higher FeO^*/MgO ratio and lower TiO_2 content (Fig. 1).

The basalts recovered by drill from the Manihiki Plateau (Jackson et al., 1976) and the Ontong-Java Plateau (Stoesser, 1975) have the same FeO^*/MgO ratio and TiO_2 content as B-type and A-type basalts, respectively, whereas glass of dredged basalt from the Danger Island Troughs in the Manihiki Plateau (Clague, 1976) is more depleted in TiO_2 (Fig. 1). MacGregor (1969) reported that the TiO_2 concentration of a eutectic melt in the system $\text{MgO}-\text{TiO}_2-\text{SiO}_2$ increases with pressure, and he suggested that the TiO_2 content of basaltic liquids is a function of the depth at which partial melting occurs. From the result of wet chemical and XMA analyses of glass, the basalt from Site 462 is a quartz-normative and strongly hypersthene-normative tholeiite. The Manihiki basalts are also quartz-norma-

tive or strongly hypersthene-normative (Jackson et al., 1976; Clague, 1976).

Experimental evidence (Green and Ringwood, 1967) suggests that quartz-normative and strongly hypersthene-normative basaltic magma can form in equilibrium with wall rocks only at very shallow depths (pressures of 5 kbar or less). Consequently, the chemistry of the Hole 462 basalt (probably also the Ontong-Java Plateau basalt) indicates that the basaltic liquids were generated at shallower depths than ocean-ridge tholeiite, as Clague (1976) supposed for the Manihiki Plateau basalt.

The Hole 462A material is depleted in Na_2O and extremely depleted in K_2O compared with ocean-ridge tholeiites such as those reported widely in the DSDP *Initial Reports* of previous legs, and elsewhere. The major element abundance and variation patterns are partly due to alteration, but the content of TiO_2 , Na_2O , and K_2O will be increased with continuing alteration, whereas the basalt of Hole 462A is different from a Hawaiian tholeiite, a typical basalt of hot-spot type, in lower K_2O and TiO_2 content. Fujii et al. (this volume) report that the basalt of Hole 462A is distinguished from normal ocean-ridge tholeiite by its higher $\text{Sr}^{87}/\text{Sr}^{86}$ ratio (0.70370 ± 0.00011), and from various oceanic-island basalts by a lower Rb/Sr ratio.

From this evidence, the chemical compositions of the sill-pillow complex from Hole 462A are significantly different from ocean-ridge tholeiite and Hawaiian tholeiite, but very similar to the Manihiki Plateau basalt.

MINERALOGY OF HOLE 462A

From observation of about 300 thin sections, we find that the basalts from Hole 462A are microdolerite, plagioclase-clinopyroxene phyric basalt, and aphyric basalt, with minor amounts of granophyre.

Microdolerite with subophitic texture occurs in the interior of basalt sills (Plate 1, Fig. 4) and partly in pillow basalts. Its mineral assemblage is plagioclase, augite, and magnetite, occasionally pigeonite. Pigeonite occurs only in Core 69, Section 2, 68–72 cm. This dolerite is commonly composed of phenocrysts to microphenocrysts of subhedral plagioclase (up to 1 mm, 2–10%) and euhedral augite (up to 0.8 mm, 2–7%), and microlites of subhedral to euhedral plagioclase (<0.3 mm, 30–40%), subhedral augite (<0.4 mm, 30–40%), and angular magnetite (<0.2 mm, 4–8%). Microphenocrysts of skeletal magnetite occasionally are observed. Alteration products such as smectite, chlorite, calcite, zeolite, and pyrite commonly are observed in veins. Several percent of clinopyroxene are usually altered to clay minerals.

Plagioclase-augite phyric basalts with hyalopilitic to intersertal texture occur next to the interiors of basalt sills and pillow basalts. This basalt is composed of microphenocrysts to phenocrysts of plagioclase (up to 1 mm, 1–3%) and augite (up to 1 mm, 1–3%), and microlites of plagioclase (<0.3 mm, 30–40%), augite (<0.3 mm, 10–20%), and magnetite (<0.2 mm, 5–10%), and interstitial glass (30–40%). Microphenocrysts of subhedral plagioclase and augite are scattered in a matrix of glass, together with microlites of subhedral to spherulitic plagioclase, subhedral to euhedral augite, and partly dust-like magnetite. Some alteration products as microdolerite are present in plagioclase-augite phyric basalt.

Aphyric basalt occurs in chilled margins of basalt sills and pillow basalts. The chilled margins of basalt sills are always strongly altered, but fresh, brown, opaque glass layers including some microphenocrysts commonly are observed in the chilled margins of pillow basalts. From the mineral assemblage in the brown opaque glass, two types are identified: a spinel, olivine, and plagioclase type, and an augite and plagioclase type. Augite and plagioclase commonly occur as aggregates. Glass analyses are presented in Table 2.

Granophyre schlieren occur in interiors of thick basalt sills. Granophyre schlieren are made of phenocrysts of subhedral to euhedral plagioclase (0.5–0.7 mm, 10–15%), subhedral to euhedral augite (1–1.2 mm, 7–15%), and angular, skeletal magnetite (1 mm, 5%), and microlites of euhedral to subhedral plagioclase (<0.4 mm, 30–40%), subhedral augite (<0.4 mm, 30–40%), and angular magnetite (<0.4 mm, 5–8%), together with accessory minerals of quartz-alkali feldspar intergrowth (micropegmatite), kaersutite, and apatite. Kaersutite may have crystallized during a final stage. Large skeletal magnetite occupies the interstices between plagioclase and augite, so it might have crystallized at a later stage, as a result of a drastic change in oxygen fugacity. Veins are commonly filled with chlorite, pyrite, and zeolite.

Table 2. Chemical composition and CIPW norms of glass from Hole 462A.

Component	47-3, 14-17 cm	48-2	62-2, 128-132 cm	69-2, 68-72 cm
SiO ₂	51.44	50.33	50.74	49.91
TiO ₂	1.00	0.92	0.93	1.07
Al ₂ O ₃	14.02	14.11	13.78	13.74
Fe ₂ O ₃	1.19	1.27	1.18	1.24
FeO	9.63	10.26	9.52	10.07
MnO	0.18	0.13	0.13	0.13
MgO	7.05	8.05	7.67	7.73
CaO	12.52	12.24	12.61	12.17
Na ₂ O	1.84	2.12	1.91	2.14
K ₂ O	0.09	0.08	0.09	0.09
NiO	0.00	0.00	0.00	0.00
Cr ₂ O ₃	0.05	0.05	0.05	0.04
Total	99.01	99.56	98.61	98.33
Q	3.08	0.00	1.23	0.00
Or	0.54	0.48	0.54	0.54
Ab	15.73	18.03	16.40	18.42
An	30.04	28.89	29.18	28.10
Ne	0.00	0.00	0.00	0.00
Wo	13.66	13.42	14.32	13.91
En	7.08	7.13	7.70	7.38
Fs	6.21	5.87	6.14	6.11
En	10.66	10.65	11.68	10.82
Fs	9.34	8.78	9.30	8.96
Fo	0.00	1.66	0.00	0.97
Fa	0.00	1.50	0.00	0.89
Mt	1.74	1.85	1.74	1.83
Il	1.92	1.76	1.79	2.07

Note: $Fe^{3+}/Fe^{2+} + Fe^{3+} = 0.1$.

Spinel

Spinel is observed only in brown opaque glass layers of pillow basalt of B type. Morphologically, the spinels occur as euhedral octahedra, typically 10 to 30 μ m in diameter, reaching a maximum width of 50 μ m. Solitary crystals can be found in glass, but most spinels are either included in olivine or attached to olivine rims (Plate 1, Figs. 1 and 2). The analyses were recast in structural formulas on the basis of four oxygens. Total Fe was partitioned between A and B sites as Fe²⁺ and Fe³⁺ in the proportions required for stoichiometry (Finger, 1972), yielding an estimation of the amount of ferric ion in the spinel. Representative microprobe analyses of spinels and their structural formulas are presented in Table 3. The spinels from Hole 462A are characterized by a higher Cr/(Cr + Al) ratio (0.54–0.73) and a lower Mg/(Mg + Fe) ratio (0.49–0.54) (Table 3). The TiO₂ contents of the spinels range from 0.5 to 0.7%. Zoning of spinel is observed in Core 62, Section 2, 128–132 cm; a decrease in Cr/(Cr + Al) from core to rim and an increase in Mg/(Mg + Fe²⁺) from core to rim.

The distinction between the spinels from Hole 462A and MAR is clearly revealed by a compositional plot of Cr/(Cr + Al) vs. Mg/(Mg + Fe²⁺) (Fig. 2), and Fe³⁺/(Cr + Al + Fe³⁺) vs. Mg/(Mg + Fe²⁺) (Fig. 3). Sigurdson and Schilling (1976) divided the spinels from MAR into three types: magnesiocromite (Mg > Fe²⁺, Cr > Al), titaniferous magnesiocromite (Mg > Fe²⁺, Cr >

Table 3. Chemical composition of spinel from Hole 462 (analyzed by XMA).

Component	47-3, 14-17 cm				48-2, 106-109 cm				62-2, 128-132 cm					47-3, 14-17 cm	
	(core)	(rim)	(core)	(core)	(core)	(rim)	(core)	(core)	(core)	(core)	(core)	(core)			
SiO ₂	0.000	0.000	0.000	0.000	0.002	0.069	0.228	0.007	0.051	0.118	0.365	0.099	0.171	0.079	0.099
Al ₂ O ₃	19.641	19.353	19.046	21.258	19.298	17.042	19.112	19.013	17.664	14.044	19.805	13.307	12.800	12.136	13.307
TiO ₂	0.688	0.629	0.686	0.714	0.788	0.679	0.700	0.783	0.665	0.453	0.762	0.561	0.555	0.478	0.561
Fe ₂ O ₃	8.148	8.149	8.715	8.634	8.566	8.650	9.107	9.547	9.123	7.223	8.786	7.548	7.553	6.114	7.548
FeO	18.858	18.907	18.615	18.340	19.012	18.790	18.198	18.563	18.658	18.413	18.162	18.500	18.249	18.634	18.500
MnO	0.000	0.000	—	—	0.539	0.655	0.557	0.516	0.662	0.589	0.475	0.575	0.616	0.583	0.575
MgO	11.961	11.895	12.065	12.254	11.444	11.325	11.443	11.896	11.278	10.616	11.538	10.785	10.594	10.011	10.785
CaO	0.084	0.111	0.126	0.074	0.033	0.050	0.168	0.199	0.084	0.081	0.145	0.144	0.187	0.068	0.144
Na ₂ O	0.000	0.000	—	—	0.000	0.000	0.025	0.000	0.000	0.000	0.000	0.022	0.003	0.000	0.022
K ₂ O	0.000	0.000	—	—	0.000	0.000	0.018	0.002	0.014	0.000	0.015	0.016	0.011	0.013	0.016
Cr ₂ O ₃	40.641	40.803	40.358	37.154	39.794	42.700	38.708	39.688	40.421	46.973	38.930	47.875	47.927	49.762	47.875
NiO	0.077	0.000	0.070	0.049	0.134	0.127	0.000	0.200	0.107	0.313	0.000	0.046	0.006	0.236	0.046
Total	100.155	100.509	99.682	98.477	99.609	100.087	98.265	100.415	98.727	98.823	98.982	99.477	98.732	98.114	99.477
Cations (O = 4)															
Si	0.0000	0.0000	0.0000	0.0000	0.0001	0.0023	0.0075	0.0002	0.0017	0.0040	0.0119	0.0033	0.0058	0.0027	0.0033
Al	0.7476	0.7394	0.7308	0.8152	0.7427	0.6600	0.7445	0.7280	0.6923	0.5567	0.7615	0.5260	0.5107	0.4881	0.5260
Ti	0.0167	0.0153	0.0168	0.0175	0.0194	0.0168	0.0174	0.0191	0.0166	0.0115	0.0187	0.0141	0.0141	0.0123	0.0141
Fe	0.1980	0.1989	0.2135	0.2114	0.2105	0.2139	0.2265	0.2334	0.2283	0.1828	0.2157	0.1905	0.1924	0.1570	0.1905
Fe	0.5090	0.5125	0.5065	0.4987	0.5188	0.5160	0.5027	0.5040	0.5185	0.5175	0.4951	0.5185	0.5163	0.5317	0.5185
Mn	0.000	0.000	—	—	0.0149	0.0182	0.0156	0.0142	0.0186	0.0168	0.0131	0.0163	0.0177	0.0168	0.0163
Mg	0.5759	0.5752	0.5856	0.5944	0.5571	0.5548	0.5639	0.5762	0.5591	0.5322	0.5611	0.5392	0.5347	0.5093	0.5392
Ca	0.0029	0.0038	0.0044	0.0026	0.0011	0.0018	0.0059	0.0069	0.0030	0.0029	0.0051	0.0052	0.0068	0.0025	0.0052
Na	0.0000	0.0000	—	—	0.0000	0.0000	0.0016	0.0000	0.0000	0.0000	0.0000	0.0014	0.0002	0.0000	0.0014
K	0.0000	0.0000	—	—	0.0000	0.0000	0.0008	0.0001	0.0006	0.0000	0.0006	0.0007	0.0005	0.0006	0.0007
Cr	1.0377	1.0464	1.0389	0.9559	1.0274	1.1093	1.0116	1.0195	1.0628	1.2490	1.0041	1.2694	1.2828	1.3426	1.2694
Ni	0.0020	0.0000	0.0018	0.0013	0.0035	0.0034	0.0000	0.0052	0.0029	0.0085	0.0000	0.0012	0.0018	0.0065	0.0012
Cr/(Cr + Al)	0.5812	0.5857	0.5870	0.5397	0.5804	0.6270	0.5760	0.5834	0.6055	0.6917	0.5687	0.7070	0.7152	0.7334	0.7070
Mg/(Mg + Fe)	0.5308	0.5288	0.5362	0.5438	0.5178	0.5181	0.5287	0.5334	0.5188	0.5070	0.5312	0.5098	0.5088	0.4892	0.5390
Fe ³⁺ /(Cr + Al + Fe ³⁺)	0.0998	0.1002	0.1077	0.1066	0.1063	0.1079	0.1142	0.1178	0.1151	0.0919	0.1087	0.0959	0.0969	0.0790	0.1035

Al, TiO₂ > 0.5 wt. %), and chromian spinel (Mg > Fe²⁺, Al > Cr). Spinel from Hole 462A have lower Mg/(Mg + Fe²⁺) and Cr/(Cr + Al) ratios compared to the three spinel types from MAR. Also, Hole 462A spinels have a higher Fe³⁺/(Cr + Al + Fe³⁺) ratio than magnesiochromites and chromian spinels, and are approximately similar to titaniferous magnesiochromites. Titaniferous magnesiochromites occur in olivine basalt with distinctly alkaline affinities. However, basalt from Hole 462A is depleted in alkalis and TiO₂. Spinel from the Manihiki Plateau also are characterized by a higher Cr/(Cr + Al) ratio (0.68–0.78) (Clague, 1976). Spinel from the Manihiki basalt with lesser magnesium content (MgO 9 wt. %) has Cr/(Cr + Al) (0.68 avg.) and Mg/(Mg + Fe²⁺) (0.53) ratios similar to those of spinel from Hole 462A. The FeO*/MgO ratio of phenocryst-free glass of the Manihiki Plateau is also similar to that of glass of Hole 462A. Moreover, the Fe³⁺/(Fe³⁺ + Al + Cr) ratio and TiO₂ content are very similar to those of Hole 462A spinel.

The glass of spinel-bearing lavas has an FeO*/(FeO* + MgO) ratio of 0.58 to 0.60 (Table 2), and a Cr content greater than 150 ppm. The occurrence of spinel in MAR basalt from the Azores region (30–40°N) is restricted to lavas with an FeO*/(FeO* + MgO) ratio less than 0.575, i.e., the least-fractionated basalts (Sigurdsson and Schilling, 1976), whereas spinel-free basalts of Leg 37 range in FeO*/(FeO* + MgO) from 0.54 to 0.60 (Sigurdsson, 1976). In basalts from the Nauru Basin, spinel of lower Mg/(Mg + Fe²⁺) ratio was crystallized from liquid of lower FeO*/(FeO* + MgO) ratio.

Olivine

Olivines are observed in the brown opaque glass layer of pillow basalt. The olivines occur as euhedral microphenocrysts (0.1–0.3 mm). Representative microprobe

analyses are given in Table 4. There is no significant compositional zoning in olivine, and its composition is Fo₈₃ to Fo₈₄. The Ni content of olivine is about 1100 ppm on the average.

Jackson (1969) and Evans and Wright (1972) have reported that the ratios Mg/(Fe²⁺ + Mg) in chromite and olivine are related. Compositions of coexisting olivine–spinel pairs in Hole 462A basalt, Manihiki basalt (Clague, 1976), Kilauea Iki (Evans and Wright, 1972), Stillwater (Jackson, 1969), and MAR (Sigurdsson and Schilling, 1976) are plotted in terms of the Mg/(Mg + Fe²⁺) ratio in Figure 4. On this figure, the olivines from Hole 462A basalts have a lower Mg/(Mg + Fe²⁺) ratio (0.83–0.84) and coexist with spinel of lower Mg/(Mg + Fe²⁺) ratio compared to olivine–spinel pairs from MAR basalt. In comparison with the olivine–spinel pairs of Kilauea Iki and the Manihiki Plateau, spinel from both regions has a similar Mg/(Mg + Fe²⁺) ratio; however, coexisting olivine has a higher Mg/(Mg + Fe²⁺) ratio than olivine from Hole 462A, whereas the spinel which coexists with olivine in the Stillwater basalts has a considerably lower Mg/(Mg + Fe²⁺) ratio than spinel from Hole 462A coexisting with olivine of similar composition.

Clinopyroxene

Clinopyroxene is the main constituent in both A and B types (Table 5). Trends of pyroxene crystallization of both types are similar, that is, slight Ca depletion with increasing Fe²⁺/(Fe²⁺ + Mg) ratio (Fig. 5). The same trend was noted in the clinopyroxenes in DSDP Leg 11 basalts (Mazzulo and Bence, 1976). Titanium generally increases with Fe enrichment. This increase is a reflection of the late-stage buildup of titanium in the residual liquid. The decrease in total Al is mainly a consequence of decreasing tetrahedral Al. Phenocrysts of B type are readily distinguished from groundmass clinopyroxenes

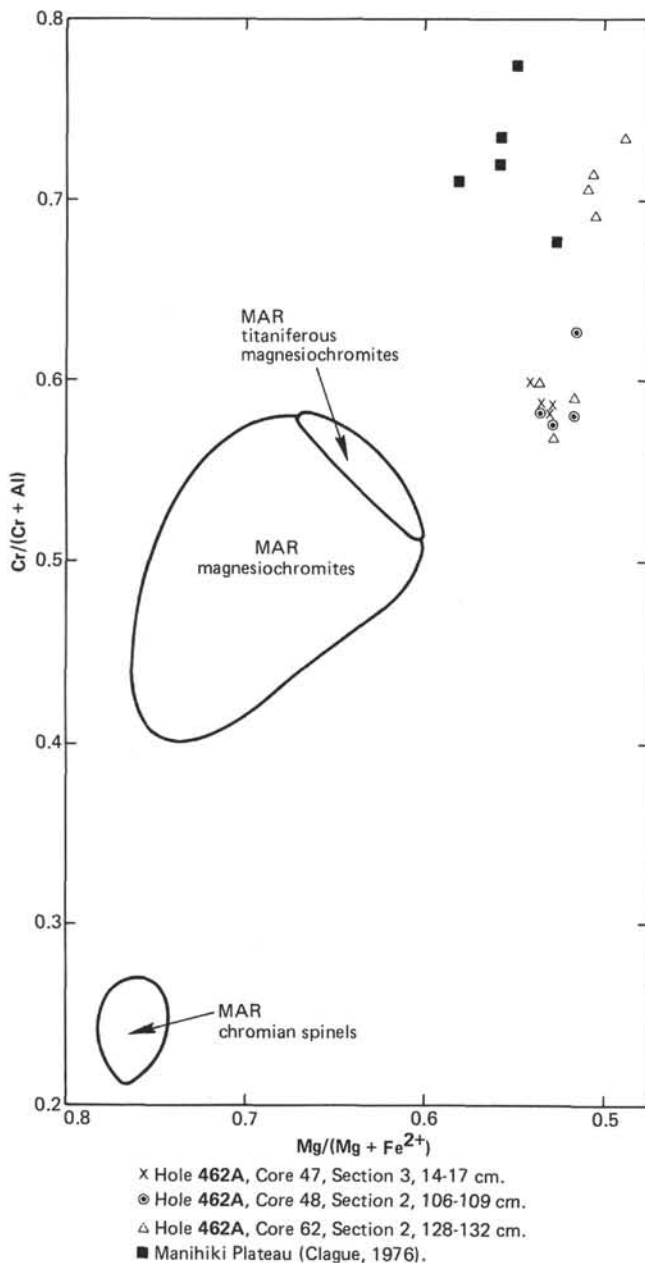


Figure 2. Spinel composition: $Cr/(Cr + Al)$ vs. $Mg/(Mg + Fe^{2+})$. Compositional fields of spinels from MAR from Sigurdsson, (1976).

by their high contents of Cr_2O_3 , but, in A type, high- Cr_2O_3 -content clinopyroxenes are observed only in core of large phenocrysts. Chromium content decreases with increase in $Fe^{2+}/(Fe^{2+} + Mg)$ (Fig. 6). Similar high-chromium clinopyroxenes are reported from Leg 15 basalts (Bence et al., 1975), and Leg 11 basalts (Ayuso and Bence, 1976). The high-chromium clinopyroxene microphenocrysts from the brown opaque glass layer of the pillow basalt never coexist with chromian spinel. The high concentrations of Cr_2O_3 in the early-crystallizing clinopyroxene reflect the absence of early-crystallizing chrome spinel, which would very rapidly deplete the melt in Cr_2O_3 .

Clinopyroxene in glass of Core 69, Section 2, seems to be a liquidus phase (Plate 1, Fig. 3). Experimental investigations on several ocean-ridge tholeiite compositions (Kushiro and Thompson, 1972) indicate that clinopyroxene can be a liquidus phase at pressures greater than about 9 kbar, and possibly at pressures as low as 5 kbar in the presence of a small (<1%) amount of water. The latter condition seems to be compatible with the shallow emplacement suggested by bulk chemistry.

Pigeonite occurs in sill interiors of type B as microphenocrysts. The Cr_2O_3 and Al_2O_3 contents are much lower than those of augites. The temperature at which pigeonites crystallize is calculated to be more than $1160^\circ C$, based on the pigeonite composition (Ishii et al., 1979).

Plagioclase

Plagioclase are main constituents in both A and B types (Table 6). Phenocryst plagioclase of B type (An_{82}) is more calcic than that of A type (An_{70}). At about An_{64-66} , the $Fe/(Fe + Mg)$ ratio increases and magnesium decreases markedly (Figs. 7 and 8). The decrease in magnesium may be related to clinopyroxene crystallization. Iron continued to rise in plagioclase up to 1.1 wt. % at a late stage (Fig. 8), reflecting its increase in the liquid. On the basis of petrography, bulk chemistry, and major- and minor-element variations, the following overall mineral paragenesis is indicated in both A and B types:

- A type: plagioclase → plagioclase + pyroxene →
plagioclase + pyroxene + magnetite →
hornblende + biotite + quartz + alkali
feldspar + titanomagnetite + (sulfide)
- B type: olivine + spinel → olivine
+ plagioclase } → plagioclase
chromium-rich pyroxene }
+ plagioclase
+ pyroxene → pyroxene
+ plagioclase + magnetite → hornblende
+ biotite + quartz + alkali feldspar
+ titanomagnetite + apatite + (sulfide)

VOLCANISM IN NAURU BASIN

The sill and pillow-basalt complex is widespread in the Nauru Basin, based on the seismic data (Voyages of *Kana Keoki* 1977; *Hakurei Maru*, 1977; and *Glomar Challenger*, this volume). The acoustic nature of the complex is characterized by low-frequency sets of smooth reflectors. The thickness of the complex may be more than 0.4 sec in two-way reflection time, estimated at more than 700 meters. The thickness of A type is less than 200 meters, and that of B type is more than 500 meters. Houtz (1976) and Houtz and Ludwig (1979) reported the seismic properties of the South Pacific Basin (including the Nauru Basin). They discussed the east-west-trending distribution of a reverberant sub-bottom layer, which might be composed of calcareous or volcanoclastic sediment. After Leg 61 drilling, it is clear that the reverberant layer in the Nauru Basin could be the volcanic complex. Such low-frequency sets of smooth reflectors are known in the Caribbean Sea

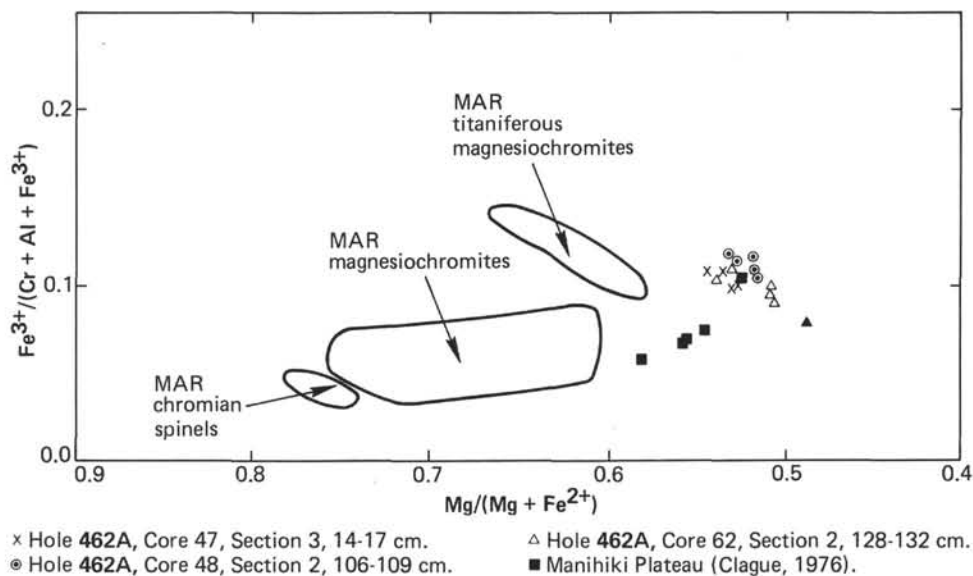


Figure 3. Spinel composition: $\text{Fe}^{3+}/(\text{Cr} + \text{Al} + \text{Fe}^{3+})$ vs. $\text{Mg}/(\text{Mg} + \text{Fe}^{2+})$. Compositional fields of spinels of MAR from Sigurdsson (1976).

Table 4. Chemical composition of olivine from Hole 462A.

Component	47-3, 14-17 cm				48-2, 106-109 cm				62-2, 128-132 cm				
SiO ₂	40.703	40.969	38.133	38.046	38.025	39.211	39.565	39.005	38.696	38.662	38.745	38.567	38.204
Al ₂ O ₃	0.083	0.067	0.021	0.026	0.071	0.065	0.106	0.064	0.081	0.091	0.079	0.069	0.060
TiO ₂	0.008	15.297	0.003	0.000	0.000	0.000	0.000	0.000	0.021	0.020	0.013	0.021	0.036
FeO	15.590	0.271	15.198	15.376	15.551	16.220	16.259	16.463	15.670	15.472	15.407	14.495	15.636
MnO	0.241	43.225	0.000	—	—	0.266	0.219	0.280	0.230	0.234	0.216	0.180	0.223
MgO	43.646	0.344	45.644	45.273	45.217	45.169	45.221	45.472	43.934	44.233	43.514	43.250	43.822
CaO	0.361	0.000	0.325	0.305	0.331	0.387	0.351	0.331	0.338	0.348	0.343	0.344	0.398
Na ₂ O	0.037	0.000	0.000	—	—	0.050	0.020	0.000	0.069	0.000	0.000	0.000	0.021
K ₂ O	0.008	0.000	0.000	—	—	0.000	0.006	0.000	0.000	0.000	0.002	0.003	0.000
Cr ₂ O ₃	0.036	0.083	0.004	0.020	0.000	0.050	0.031	0.063	0.031	0.016	0.000	0.035	0.073
NiO	0.204	0.117	0.182	0.136	0.023	0.170	0.124	0.110	0.122	0.264	0.199	0.252	0.056
Total	100.917	100.445	99.510	99.182	99.218	101.589	101.901	101.788	99.192	99.340	98.517	98.215	98.530
Cations (O = 4)													
Si	1.0144	1.0230	0.9681	0.9696	0.9690	0.9783	0.9827	0.9725	0.9863	0.9838	0.9927	0.9922	0.9812
Al	0.0025	0.0021	0.0006	0.0008	0.0021	0.0019	0.0031	0.0019	0.0024	0.0027	0.0024	0.0021	0.0018
Ti	0.0002	0.0013	0.0001	0.0000	0.0000	0.0000	0.0000	0.0000	0.0004	0.0004	0.0002	0.0004	0.0007
Fe	0.3249	0.3195	0.3227	0.3277	0.3314	0.3384	0.3377	0.3433	0.3340	0.3293	0.3301	0.3334	0.3359
Mn	0.0051	0.0057	0.0000	—	—	0.0056	0.0046	0.0059	0.0050	0.0051	0.0047	0.0039	0.0049
Mg	1.6215	1.6091	1.7275	1.7201	1.7178	1.6800	1.6744	1.6961	1.6695	1.6779	1.6621	1.6587	1.6779
Ca	0.0096	0.0092	0.0088	0.0083	0.0090	0.0103	0.0093	0.0088	0.0092	0.0095	0.0094	0.0095	0.0110
Na	0.0018	0.0000	0.0000	—	—	0.0024	0.0009	0.0000	0.0034	0.0000	0.0000	0.0000	0.0010
K	0.0002	0.0000	0.0000	—	—	0.0000	0.0002	0.0000	0.0000	0.0000	0.0001	0.0001	0.0000
Cr	0.0007	0.0016	0.0001	0.0004	0.0000	0.0010	0.0006	0.0012	0.0006	0.0003	0.0000	0.0007	0.0015
Ni	0.0041	0.0023	0.0037	0.0028	0.0005	0.0034	0.0025	0.0022	0.0025	0.0054	0.0041	0.0052	0.0012
Olivine component (mol %)													
Fo	83.49	83.43	84.26	84.00	83.83	83.23	83.22	83.12	83.33	83.59	83.43	83.26	83.32
Fa	16.51	16.57	15.94	16.00	16.17	16.77	16.78	16.88	16.67	16.41	16.57	16.74	16.68

(Talwani, Windisch, et al., 1977) and the western flank of the Atlantic Ocean (Grow and Marble, 1977).

The intraplate volcanism in the Nauru Basin represents a voluminous outpouring of magma without edifice-building. It is unclear from the seismic data whether lavas were fed from numerous extensive fissures or vents in the Nauru Basin. However, we may judge that they were from the fact that continental plateau basalt fissure eruptions generally produce much larger volumes than eruptions from localized vents. Also, the rocks from fissure eruptions are generally

quartz-normative tholeiite, whereas those from vents are alkalic (Kuno, 1969). Thus, it is concluded that the lavas might be fed from numerous fissures.

The chemical composition of the Nauru Basin basalt is significantly different from that of ocean-ridge tholeiites. Furthermore, the composition is distinguished from a Hawaiian tholeiite of typical hot-spot type, and from seamount basalts. Basalts with similar composition are recovered from the Manihiki Plateau and the Ontong-Java Plateau; they are characterized by a higher FeO^*/MgO ratio and lower TiO_2 content, and

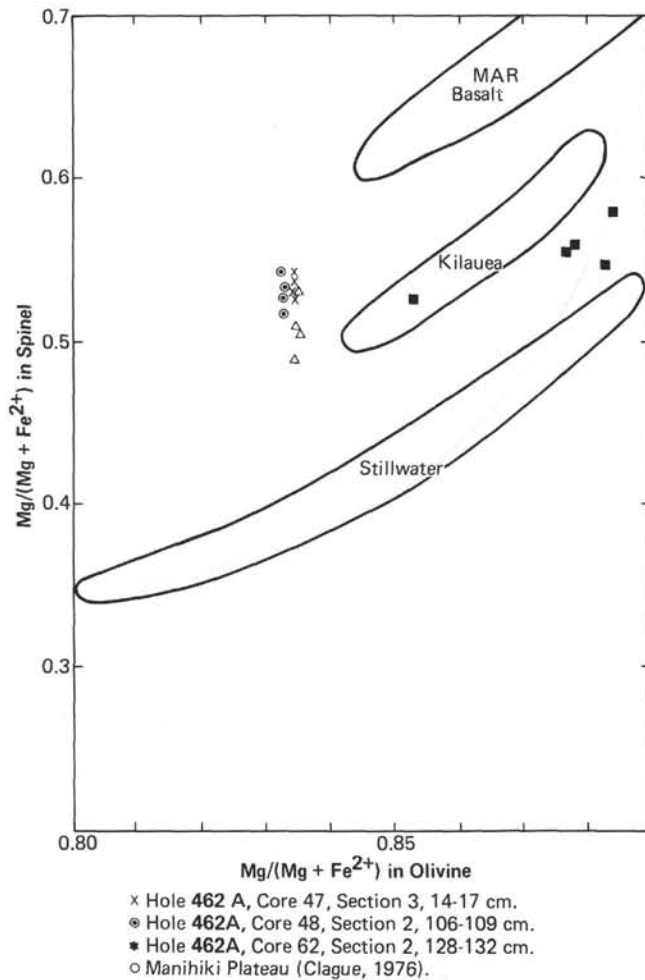


Figure 4. Composition of coexisting olivine-spinel pairs in Hole 462A basalts, plotted in terms of the $Mg/(Mg + Fe^{2+})$ ratio. MAR basalt (Sigurdsson, 1976), Kilauea (Evans and Wright, 1972), and Stillwater (Jackson, 1969) are also plotted.

they contain normative quartz and hypersthene. We propose a new name for this characteristic group of basalts—ocean-plateau tholeiite. As discussed above, ocean-plateau tholeiites may originate from shallow depths (< 5 kbar). The melting anomaly which produces such a huge volume of volcanic rocks in the Nauru Basin may cause lithospheric thinning and thickening of the lower crust, thus causing buoyant ocean floor.

There were two intraplate volcanism episodes in the Nauru Basin. The younger volcanic event, characterized by A type, occurred in the Cenomanian to Albian, whereas the older volcanic event, characterized by B type, took place in the Barremian to Valanginian. The lithologic difference between A and B types is explained by the following hypothesis: A-type volcanics, which occur as intrusions, form under conditions of less tension, so that magmas are trapped in shallow reservoirs for longer times of fractionation; B-type volcanics, which occur as extrusives and intrusives, form under tensional conditions, so that there is no time for fractionation. There is a compositional variation in A-type basalts. The degree of fractionation of olivine can be

estimated approximately from the NiO content and the $Mg/(Mg + Fe^*)$ ratio of the magma, because olivine effectively removes Ni and Mg from magma. However, there is no significant Ni variation in A-type basalt. The TiO_2 content of most calcic clinopyroxene from A type is up to 0.5 wt. %, less than that of A-type basalt. If the primitive magma contained about 1% TiO_2 , the variation of the FeO^*/MgO ratio and TiO_2 content might be explained by low-pressure fractionation of clinopyroxene with a small amount of water.

The temperature estimate based on the distribution coefficient for the partitioning of iron and magnesium between olivine and coexisting liquid (Roeder and Emslie, 1970) is approximately 1215°C. The Fe^{2+} of coexisting liquid is calculated by using a glass atomic ratio $Fe^{3+}/(Fe^{3+} + Fe^{2+})$ of 0.1, which is the minimum observed in oceanic-ridge basalt (Miyashiro et al., 1969), whereas the temperature estimate obtained by using pigeonite composition (Ishii et al., 1979) is more than 1160°C.

Winterer (1975) indicated that the Manihiki Plateau and Ontong-Java Plateau are ridges abandoned about 105 m.y. ago, in relation to the southward shift of the triple junction of the Pacific, Farallon, and Antarctic Plates, because areas of voluminous mantle melting usually occur near lithospheric triple junctions. However, the basalts from the Nauru Basin, the Manihiki Plateau, and the Ontong-Java Plateau are chemically different from ocean-ridge tholeiite. Consequently, ocean-plateau volcanism, which forms ocean plateaus or huge sill and pillow-basalt complexes, is distinguished from ocean-ridge tholeiite and hot-spot tholeiite by its chemical composition and its wide distribution. The magma might be generated at a shallow melting anomaly with considerable tension. It is thus assumed that the complex is not formed at a normal oceanic ridge. Normal oceanic basement could therefore underlie the sill and pillow-basalt complex in the Nauru Basin.

ACKNOWLEDGMENTS

We are grateful to Assoc. Prof. H. Kagami and Dr. T. Ishii for critical reading of the manuscript. We are indebted to Prof. N. Nasu and Dr. N. Fujii for critical suggestions.

REFERENCES

- Ayuso, R. A., and Bence, A. B., 1976. Upper Jurassic tholeiitic basalt from DSDP Leg 11, *J. Geophys. Res.*, 81:4305-4325.
- Bence, A. E., Papike, J. J., and Ayuso, R. A., 1975. Petrology of submarine basalts from the central Caribbean: DSDP Leg 15, *J. Geophys. Res.*, 80:4775-4803.
- Bryan, W. B., and Moore, J. G., 1977. Compositional variation of young basalts in the Mid-Atlantic rift valley near 36°49'N. *Geol. Soc. Am. Bull.*, 88:556-570.
- Burke, K., Fox, P. J., and Sengor, A. M. C., 1978. Buoyant ocean floor and the evolution of the Caribbean. *J. Geophys. Res.*, 83: 3949-3954.
- Cande, S. C., Larson, R. L., and La Brocque, J. L., 1978. Magnetic lineations in the Jurassic quiet zone. *Earth Planet. Sci. Lett.*, 41:434-440.
- Clague, D. A., 1976. Petrology of basaltic and gabbroic rocks dredged from the Danger Island Troughs, Manihiki Plateau. In Schlanger, S. O., Jackson, E. D., *Init. Repts. DSDP*, 33: Washington (U.S. Govt. Printing Office), 891-907.
- Clague, D. A., and Bunch, T. E., 1976. Formation of ferrobasalts at east Pacific midocean spreading centers. *J. Geophys. Res.*, 81: 4247-4256.

Table 5. Chemical composition of pyroxene from Hole 462A.

Component	21-1				24-3, 81-85 cm						50-2, 60-63 cm					
	Phenocryst			Groundmass	Microlite		Phenocryst			Phenocryst						
	Rim	Zoned	Core		Core	Core	Core	Core	Rim	Zoned	Core	Core				
SiO ₂	52.432	52.035	52.394	50.527	53.453	52.145	52.247	52.380	51.770	51.321	53.488	53.490	52.454	52.073	52.004	50.285
Al ₂ O ₃	1.260	2.160	1.759	1.626	1.330	1.070	1.843	1.647	1.968	2.057	1.480	1.646	1.947	3.038	2.768	2.848
TiO ₂	0.495	0.412	0.481	0.653	0.392	0.401	0.000	0.448	0.357	0.509	0.373	0.116	0.353	0.154	0.273	0.289
FeO	11.159	7.277	7.526	17.831	8.591	10.922	11.337	7.445	8.048	7.367	6.686	6.016	6.053	6.239	6.153	7.283
MnO	—	—	—	—	—	—	—	—	—	—	—	—	—	—	—	—
MgO	17.366	17.955	17.312	15.213	17.337	16.887	15.387	16.793	16.548	16.160	18.569	18.444	17.681	17.101	17.555	17.210
CaO	15.985	18.234	18.462	12.755	18.198	16.972	17.396	19.570	19.460	19.923	18.715	18.997	20.324	20.396	19.398	20.830
Na ₂ O	0.168	0.185	0.193	0.205	0.217	0.269	0.254	0.200	0.205	0.334	0.143	0.146	0.170	0.200	0.167	0.223
K ₂ O	0.000	0.000	0.000	0.000	0.004	0.000	0.020	0.018	0.059	0.000	0.000	0.000	0.018	0.000	0.000	0.003
Cr ₂ O ₃	0.000	0.365	0.562	0.046	0.180	0.027	0.007	0.171	0.365	0.575	0.185	0.423	0.671	0.690	1.052	1.110
NiO	—	—	—	—	—	—	—	—	—	—	—	—	—	—	—	—
Total	98.864	98.622	98.689	98.855	99.701	98.693	98.490	98.673	98.779	98.245	99.640	99.273	99.671	99.891	99.369	100.080
Cations (O = 6)																
Si	1.9592	1.9328	1.9476	1.9381	1.9700	1.9607	1.9706	1.9523	1.9356	1.9288	1.9588	1.9619	1.9303	1.9130	1.9164	1.8666
Al	0.0408	0.0672	0.0524	0.0619	0.0300	0.0393	0.0294	0.0477	0.0644	0.0712	0.0412	0.0381	0.0697	0.0870	0.0836	0.1246
Al	0.0147	0.0274	0.0247	0.0116	0.0278	0.0081	0.0525	0.0246	0.0223	0.0199	0.0227	0.0331	0.0147	0.0445	0.0366	0.0000
Ti	0.0139	0.0115	0.0135	0.0188	0.0109	0.0113	0.0000	0.0126	0.0100	0.0144	0.0103	0.0032	0.0098	0.0043	0.0076	0.0081
Fe	0.3488	0.2261	0.2340	0.5720	0.2648	0.3435	0.3576	0.2321	0.2517	0.2315	0.2048	0.1845	0.1863	0.1916	0.1896	0.2261
Mn	—	—	—	—	—	—	—	—	—	—	—	—	—	—	—	—
Mg	0.9674	0.9943	0.9594	0.8700	0.9525	0.9466	0.8652	0.9331	0.9224	0.9054	1.0138	1.0085	0.9699	0.9366	0.9644	0.8284
Ca	0.6400	0.7256	0.7353	0.5242	0.7186	0.6838	0.7030	0.7815	0.7796	0.8023	0.7343	0.7465	0.8013	0.8028	0.7659	0.8284
Na	0.0122	0.0133	0.0140	0.0152	0.0155	0.0196	0.0186	0.0144	0.0149	0.0243	0.0101	0.0104	0.0121	0.0143	0.0119	0.0160
K	0.0000	0.0000	0.0000	0.0000	0.0002	0.0000	0.0010	0.0009	0.0028	0.0000	0.0000	0.0000	0.0009	0.0000	0.0000	0.0001
Cr	0.0000	0.0107	0.0165	0.0014	0.0052	0.0008	0.0002	0.0050	0.0108	0.0171	0.0054	0.0123	0.0195	0.0200	0.0306	0.0326
Ni	—	—	—	—	—	—	—	—	—	—	—	—	—	—	—	—
En	49.45	51.09	49.75	44.25	49.20	47.96	44.93	47.93	47.21	46.69	51.91	52.00	49.55	48.50	50.23	47.46
Fs	17.83	11.62	12.13	29.09	13.68	17.40	18.57	11.92	12.88	11.94	10.49	9.51	9.52	9.92	9.88	11.27
Wo	32.72	37.29	38.12	26.66	37.12	34.64	36.50	40.14	39.90	41.37	37.60	38.49	40.93	41.58	39.89	41.28

Evans, B. W., and Wright, T. L., 1972. Composition of liquidus chromite from the 1959 (Kilauea Iki) and 1965 (Makaopuhi) eruptions of Kilauea Volcano, Hawaii. *Am. Mineral.*, 57:217-230.

Finger, L. W., 1972. The uncertainty in the calculated ferric iron content of a microprobe analysis. *Ann. Rept. Dir. Geophys. Lab.*, 71:600-603.

Green, D. H., and Ringwood, A. E., 1967. The genesis of basaltic magmas. *Contr. Mineral. Petrol.*, 15:103-109.

Grow, J. A., and Marble, R. G., 1977. IPOD-USGS multichannel seismic reflection profile from Cape Hatteras to the Mid-Atlantic Ridge. *Geology*, 5:625-630.

Houtz, R. E., 1976. Seismic properties of layer 2A in the Pacific. *J. Geophys. Res.*, 81:6321-6331.

Houtz, R. E., and Ludwig, W. J., 1979. Distribution of reverberant subbottom layers in the Southwest Pacific Basin. *J. Geophys. Res.*, 84:3497-3504.

Ishii, T., Takeda, H., and Yanai, K., 1979. Pyroxene geothermometry applied to a three-pyroxene achondrite from Allan Hills, Antarctica and ordinary chondrites. *Mineral. J.*, 9:460-481.

Jackson, E. D., 1969. Chemical variation in coexisting chromite and olivine in chromite zones of Stillwater Complex. *Econ. Geol. Monogr.*, 4:41-71.

Jackson, E. D., Bargar, K. E., Fabbi, B. P., et al., 1976. Petrology of the basaltic rocks drilled on Leg 33 of the Deep Sea Drilling Project. In Schlanger, S. O., Jackson, E. D., et al., *Init. Repts. DSDP*, 33: Washington (U.S. Govt. Printing Office), 571-630.

Kuno, H., 1969. Plateau basalts, the earth's crust and upper mantle. *Geophys. Monogr.*, 13:495-501.

Kushiro, I., and Thompson, R. N., 1972. Origin of some abyssal tholeiites from the Mid-Atlantic ridge. *Carnegie Inst. Washington Yearbook*, 71:403-406.

Macdonald, G. A., and Kateura, T., 1964. Chemical composition of Hawaiian lavas. *J. Petrol.*, 5:82-133.

MacGregor, A. L., 1969. The system MgO-SiO₂ and its bearing on the distribution of TiO₂ in basalts. *Am. J. Sci.*, 267-A:342-363.

Mazzulo, L. J., and Bence, A. E., 1976. Abyssal tholeiites from DSDP Leg 34: The Nazca Plate. *J. Geophys. Res.*, 81:4327-4351.

Table 5. (Continued).

50-2, 60-63 cm			65-1, 59-61 cm									69-2, 68-72 cm			
Phenocryst	Microcline		Groundmass	Groundmass	Groundmass	Microphenocryst	Microphenocryst			Microphenocryst					
	Core	Rim					Rim	Zoned	Core	Core	Core				
51.091	50.779	52.213	49.422	49.613	49.546	54.360	52.422	53.732	50.986	51.761	52.437	52.761	52.327	50.421	50.448
2.870	1.770	2.061	1.175	1.996	2.242	1.306	0.793	0.804	2.236	3.014	3.164	3.183	2.002	3.715	3.808
0.292	0.604	0.518	0.620	0.761	0.760	0.317	0.819	0.171	0.594	0.647	0.641	0.280	0.279	0.548	0.670
6.390	17.583	13.211	25.421	16.954	16.144	12.427	18.563	17.464	13.453	9.202	8.336	6.609	6.658	6.087	7.312
—	—	—	—	—	—	—	—	—	—	—	—	—	0.180	0.165	0.144
17.328	16.978	18.003	8.766	15.749	15.283	23.899	20.449	20.007n	16.216	17.567	17.115	16.539	18.750	16.918	17.002
20.275	10.999	13.031	16.156	13.759	14.478	6.712	5.437	7.140	15.096	16.470	17.769	19.358	17.980	20.278	19.523
0.153	0.194	0.147	0.176	0.142	0.259	0.081	0.622	0.268	0.218	0.175	0.181	0.138	0.711	0.225	0.191
0.000	0.013	0.002	0.000	0.000	0.000	0.000	0.082	0.049	0.007	0.000	0.000	0.000	0.004	0.000	0.010
0.920	0.000	0.000	0.000	0.000	0.000	0.001	0.019	0.022	0.008	0.082	0.243	0.678	0.358	0.914	0.548
—	—	—	—	—	—	0.000	—	—	—	—	—	—	0.021	0.000	0.000
99.419	98.919	99.215	10- 1.736	98.759	98.712	99.104	99.205	99.657	98.814	98.918	99.886	99.546	98.749	99.273	99.677
1.8929	—	—	—	—	—	1.9791	1.9660	1.9957	1.9283	1.9216	1.9252	1.9370	1.9358	1.8707	1.8684
0.1071	1.9333	1.9472	1.9298	1.9068	1.9026	0.0209	0.0340	0.0043	0.0717	0.0784	0.0748	0.0630	0.0642	0.1293	0.1316
0.0182	0.0667	0.0528	0.0541	0.0904	0.0974	0.0352	0.0010	0.0309	0.0280	0.0535	0.0621	0.0747	0.0231	0.0031	0.0346
0.0081	0.0127	0.0378	0.0000	0.0000	0.0041	0.0087	0.0231	0.0048	0.0169	0.0181	0.0177	0.0077	0.0083	0.0153	0.0187
0.1980	0.0173	0.0145	0.0182	0.0158	0.0220	0.3784	0.5822	0.5425	0.4255	0.2857	0.2559	0.2029	0.2060	0.1889	0.2265
—	0.5599	0.4120	0.8301	0.5449	0.5185	—	—	—	—	—	—	—	0.0056	0.0052	0.0045
0.8088	—	—	—	—	—	1.2972	1.1433	1.1078	0.9143	0.9722	0.9368	0.9052	1.0341	0.9358	0.9398
0.8088	0.9636	1.0026	0.5103	0.9024	0.8749	0.2618	0.2185	0.2841	0.6117	0.6551	0.6990	0.7614	0.7127	0.8061	0.7747
0.0110	0.4487	0.5207	0.6759	0.5666	0.5957	0.0057	0.0452	0.0193	0.0160	0.0126	0.0129	0.0098	0.0123	0.0162	0.0137
0.0000	0.0143	0.0106	0.0134	0.0106	0.0193	0.0000	0.0039	0.0023	0.0003	0.0000	0.0000	0.0000	0.0002	0.0000	0.0005
0.0269	0.0006	0.0001	0.0000	0.0000	0.0000	0.0000	0.0006	0.0006	0.0002	0.0024	0.0071	0.0193	0.0105	0.0268	0.0160
—	—	—	—	—	—	—	—	—	—	—	—	—	0.0006	0.0000	0.0000
48.73	48.86	51.81	25.31	44.81	43.98	66.96	58.81	57.27	46.85	50.82	49.52	48.42	52.95	48.47	48.42
10.09	28.39	21.29	41.17	27.06	26.07	19.53	29.95	28.04	21.80	14.93	13.53	10.85	10.55	9.78	11.67
41.18	22.75	26.90	33.52	28.13	29.95	13.51	11.24	14.69	31.35	34.25	36.95	40.73	36.50	41.75	39.91

Miyashiro, A., Shido, F., and Ewing, M., 1969. Diversity and origin of abyssal tholeiite from the Mid-Atlantic Ridge near 24 and 30 north latitude. *Contr. Mineral. Petrol.*, 23:38-52.

Roeder, P. L., and Emslie, R. F., 1970. Olivine liquid equilibrium. *Contr. Mineral. Petrol.*, 29:275-289.

Sclater, J., and Francheteau, J., 1970. The implications of terrestrial heat flow observations on current tectonic and geochemical models of the crust and upper mantle of the earth. *Geophys. J. Royal Astron. Soc.*, 20:509-542.

Sigurdsson, H., 1976. Spinel in Leg 37 basalt and peridotites: phase chemistry and zoning. In Karig, D. E., Ingle, J. C., Jr., et al., *Init. Repts. DSDP*, 31: Washington (U.S. Govt. Printing Office), 883-891.

Sigurdsson, H., and Schilling, J.-G., 1976. Spinel in Mid-Atlantic Ridge basalts: chemistry and occurrence. *Earth Planet. Sci. Lett.*, 29:7-20.

Stoeser, D. B., 1975. Igneous rocks from Leg 30 of the Deep Sea Drilling Project. In Andrews, J. E., Packham, G., et al., *Init. Repts. DSDP*, 30: Washington (U.S. Govt. Printing Office), 401-414.

Subramanian, A. P., and Sahasrabudhe, 1964. Geology of greater Bombay and Aurangabad-Ellora-Ajanta area. *Internat. Geol. Congr., 22nd, India, Guide to Excursions Nos. A-13 and C-10*, 1-12.

Talwani, M., Windisch, C. C., Stoffa, T. L., et al., 1977. Multi-channel seismic study in the Venezuelan Basin and the Curacao Ridge. In Talwani, M., and Pitman, W. C. (Eds.), *Island Arcs, Deep Sea Trenches and Back-Arc Basins*: Washington (Am. Geophys. Union), pp. 83-97.

Walker, F., and Poldervaart, A., 1949. Karroo dolerites of the Union of South Africa. *Geol. Soc. Am. Bull.*, 60:591-701.

Winterer, E. L., 1975. Bathymetry and regional tectonic setting of the Line Islands Chain. In Schlanger, S. O., Jackson, E. D., et al., *Init. Repts. DSDP*, 33: Washington (U.S. Govt. Printing Office), 731-747.

Worzel, J. L., Bryant, W., et al., 1973. *Init. Repts. DSDP*, 10: Washington (U.S. Govt. Printing Office).

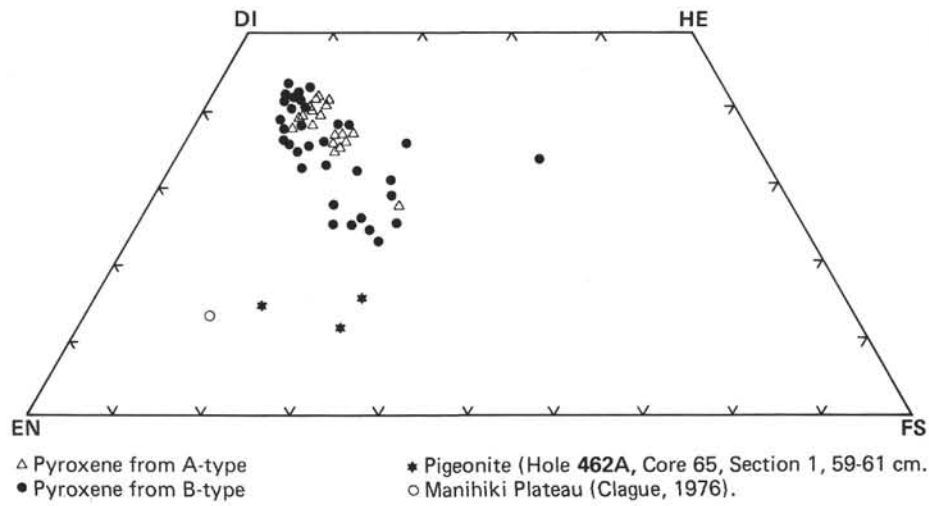


Figure 5. Pyroxene analyses from Hole 462A plotted on the pyroxene quadrilateral.

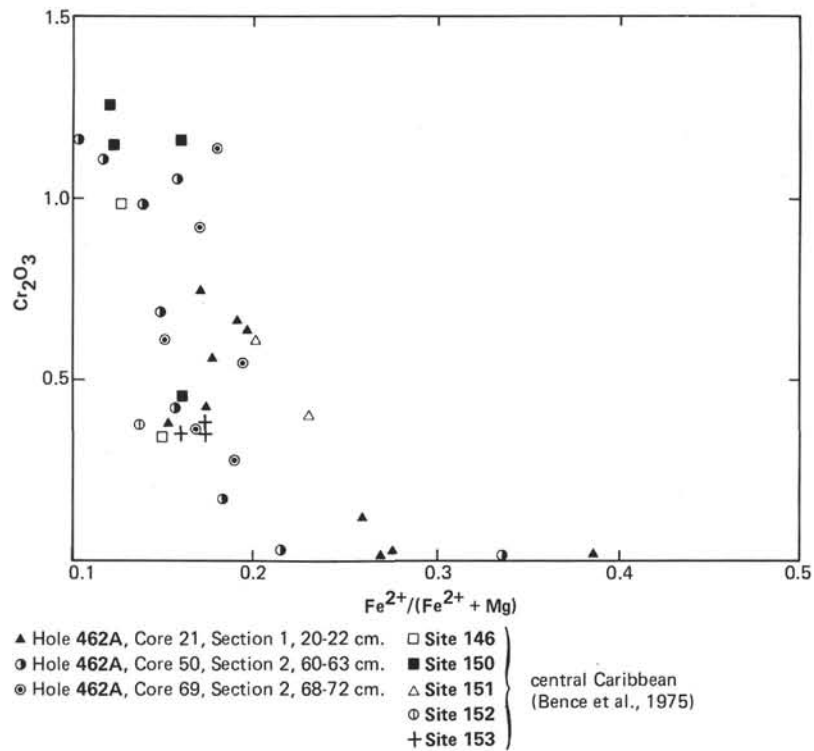


Figure 6. Variation of Cr with the $Fe^{2+}/(Fe^{2+} + Mg)$ ratio of clinopyroxenes, Hole 462A.

Table 6. Chemical composition of plagioclase from Hole 462A.

Component	21-1		24-3, 81-85 cm			47-3, 14-17 cm		48-2, 106-109 cm		50-2, 60-63 cm				62-2, 128-132 cm		65-1, 59-61 cm				69-2, 68-72 cm	
	Microlite		Microlite			Microphenocryst		Microphenocryst		Phenocryst		Microphenocryst		Microphenocryst	Phenocryst	Phenocryst				Microphenocryst	
								Core	Core	Core	Rim	Core	Rim	Core	Core	Core		Rim	Core	Core	
SiO ₂	52.233	50.432	51.018	52.898	53.686	55.314	50.560	49.282	48.478	47.744	51.561	52.018	52.268	47.487	47.033	46.411	51.769	53.801	56.216	46.571	48.910
Al ₂ O ₃	28.819	29.188	28.458	28.411	27.177	26.360	31.981	30.518	31.888	32.535	29.223	29.335	28.624	31.325	31.973	33.064	29.990	28.612	27.632	31.627	30.217
TiO ₂	0.007	0.059	0.088	0.076	0.030	0.063	—	0.000	0.000	0.168	0.069	0.070	0.000	0.030	0.009	0.032	1.454	0.113	0.035	0.031	0.056
FeO	0.606	0.636	0.594	0.802	0.885	0.772	0.805	0.582	0.630	0.770	1.050	0.886	1.111	0.610	0.707	0.648	0.945	1.054	1.041	0.821	0.864
MnO	—	—	—	—	—	—	—	0.000	0.020	—	—	—	—	0.003	0.000	—	—	—	—	0.000	0.000
MgO	0.251	0.221	0.225	0.149	0.137	0.091	0.371	0.291	0.257	0.213	0.228	0.203	0.153	0.284	0.276	0.204	0.210	0.162	0.055	0.357	0.859
CaO	13.763	14.504	13.986	13.276	12.056	10.101	15.686	15.101	16.710	16.694	13.909	13.467	13.003	16.684	17.449	16.947	12.698	11.958	10.278	15.955	14.977
Na ₂ O	3.696	3.393	3.558	4.094	4.898	5.684	2.639	2.863	2.338	2.115	3.930	3.737	4.307	2.178	2.005	1.925	4.027	4.894	5.790	2.585	3.163
K ₂ O	0.090	0.029	0.034	0.041	0.123	0.099	0.014	0.028	0.025	0.008	0.003	0.018	0.027	0.16	0.003	0.008	0.034	0.042	0.096	0.022	0.049
Cr ₂ O ₃	0.053	0.079	0.066	0.029	0.022	0.000	0.070	0.000	0.000	0.000	0.000	0.000	0.000	0.000	0.014	0.023	0.003	0.000	—	0.000	0.000
NiO	—	—	—	—	—	0.000	—	0.000	0.000	—	—	—	—	0.000	0.000	—	—	—	—	0.035	0.000
Total	99.521	98.540	98.027	99.778	99.042	98.45	102.192	98.665	100.345	100.248	99.974	99.734	99.492	98.616	99.469	99.261	101.130	100.637	101.143	98.004	98.595
Cations (O = 8)																					
Si	2.3911	2.3409	2.3751	2.4046	2.4611	2.5380	2.2668	2.2868	2.2232	2.1931	2.3595	2.3765	2.3973	2.2173	2.1842	2.1558	2.3348	2.4308	2.5128	2.1920	2.2785
Al	1.5549	1.5967	1.5614	1.5217	1.4680	1.4130	1.6899	1.6689	1.7236	1.7613	1.5761	1.5795	1.5473	1.7239	1.7500	1.8102	1.5941	1.5236	1.4557	1.7545	1.6590
Ti	0.0002	0.0021	0.0031	0.0026	0.0020	0.0011	0.0021	0.0000	0.0000	0.0058	0.0024	0.0024	0.0000	0.0010	0.0003	0.0011	0.0493	0.0038	0.0012	0.0011	0.0020
Fe	0.0232	0.0247	0.0231	0.0305	0.0339	0.0296	0.0302	0.0226	0.0242	0.0296	0.0402	0.0339	0.0426	0.0238	0.0275	0.0252	0.0356	0.0398	0.0389	0.0323	0.0336
Mn	—	—	—	—	—	—	0.0000	0.0000	0.0008	—	—	—	—	0.0001	0.0000	—	—	—	—	0.0000	0.0000
Mg	0.0171	0.0153	0.0156	0.0101	0.0094	0.0062	0.0248	0.0201	0.0176	0.0146	0.0156	0.0138	0.0104	0.0198	0.0191	0.0141	0.0141	0.0109	0.0037	0.0251	0.0250
Ca	0.6750	0.7213	0.6976	0.6466	0.5922	0.4965	0.7535	0.7508	0.8211	0.8216	0.6820	0.6592	0.6390	0.8347	0.8682	0.8434	0.6136	0.5789	0.4922	0.8046	0.7475
Na	0.3281	0.3053	0.2211	0.3610	0.4354	0.5056	0.2294	0.2576	0.2079	0.1884	0.3487	0.3311	0.3830	0.1972	0.1805	0.1734	0.3521	0.4288	0.5018	0.2360	0.2857
K	0.0053	0.0017	0.0020	0.0023	0.0072	0.0058	0.0008	0.0016	0.0014	0.0005	0.0002	0.0011	0.0016	0.0009	0.0002	0.0005	0.0020	0.0024	0.0055	0.0013	0.0029
Cr	0.0019	0.0029	0.0024	0.0001	0.0008	0.0000	0.0025	0.0000	0.0000	0.0000	0.0000	0.0000	0.0000	0.0000	0.0005	0.0008	0.0001	0.0000	0.0000	0.0000	0.0000
Ni	—	—	—	—	—	—	—	0.0000	0.0000	—	—	—	—	0.0000	0.0005	—	—	—	—	0.0013	0.0000
Plagioclase component (mol %)																					
An	66.94	70.14	68.35	64.03	57.23	49.26	76.60	73.34	79.69	81.31	66.17	66.49	62.43	80.82	82.77	82.91	63.41	57.31	49.24	77.23	72.15
Ab	32.54	29.69	31.46	35.75	42.08	50.16	23.32	25.50	20.18	18.64	33.83	33.40	37.42	19.09	17.21	17.05	36.39	42.45	50.21	22.65	0.28
Or	0.52	0.17	0.19	0.22	0.69	0.58	0.08	0.16	0.23	0.05	0.00	0.11	0.15	0.09	0.02	0.04	0.20	0.24	0.55	0.12	27.57
Fe/(Fe + Mg)	0.576	0.618	0.597	0.751	0.783	0.827	0.549	0.529	0.579	0.670	0.720	0.711	0.816	0.546	0.590	0.641	0.716	0.785	0.913	0.563	0.573

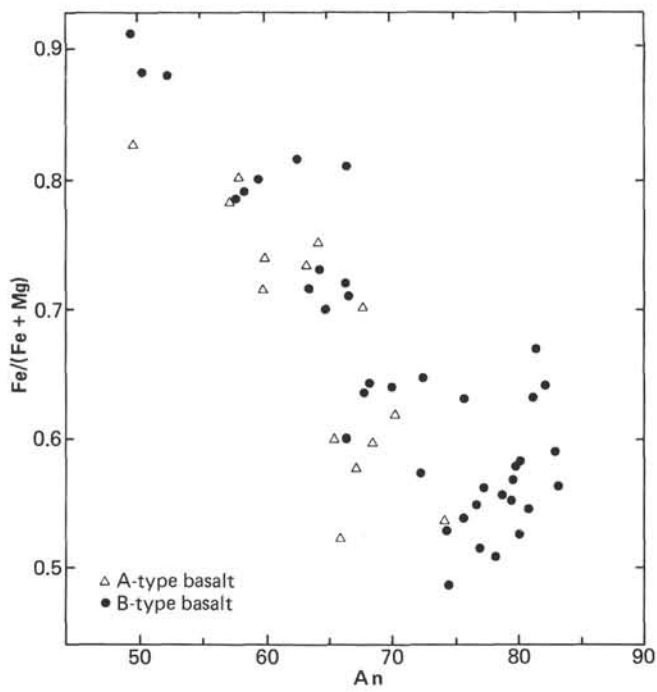


Figure 7. Plagioclase An content plotted as a function of the Fe/(Fe + Mg) ratio.

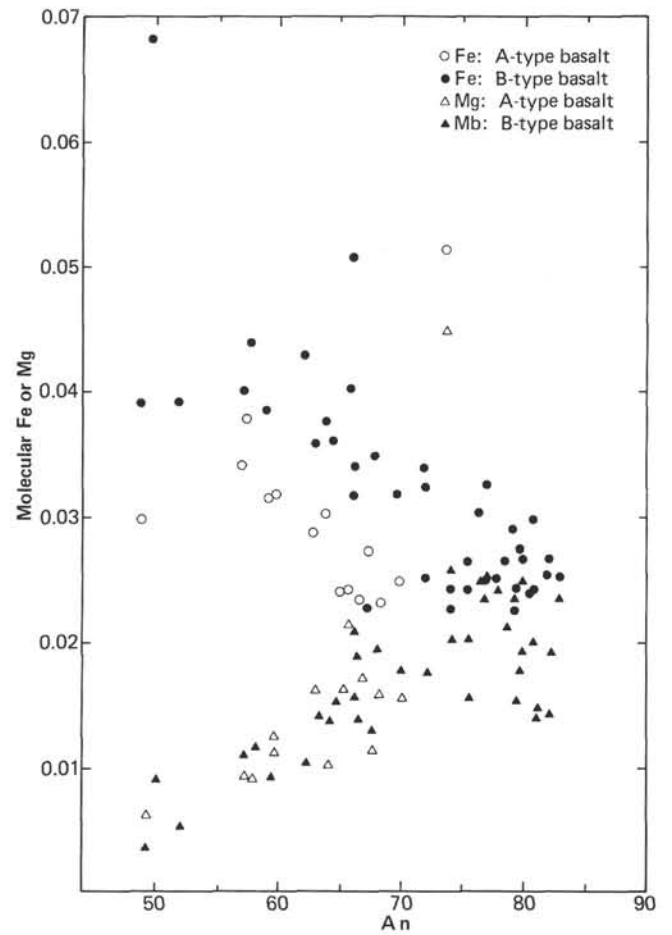


Figure 8. Plagioclase An content plotted as a function of Fe and Mg content.

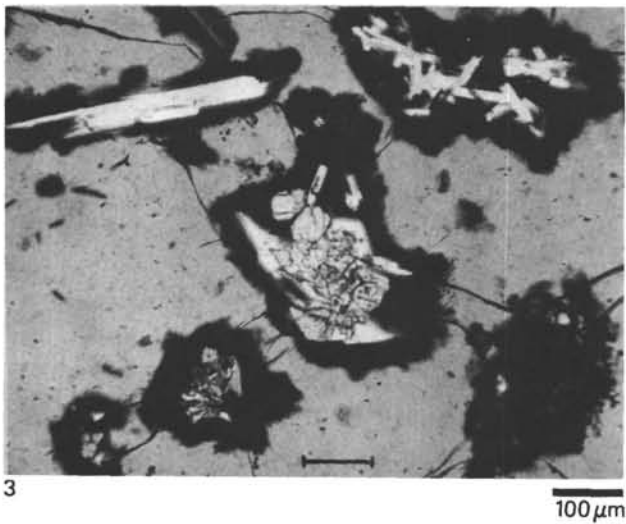
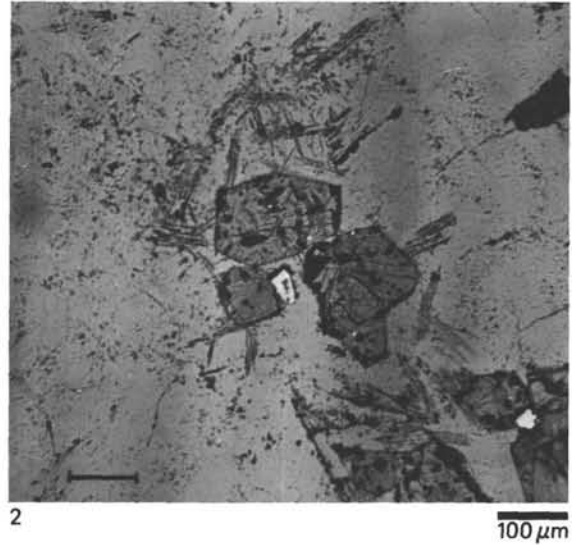
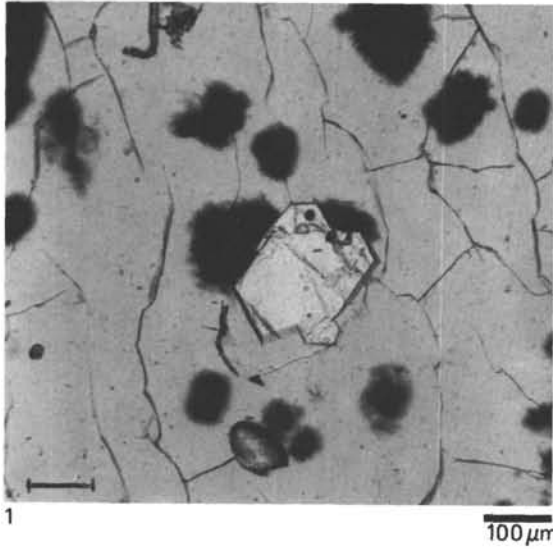


Plate 1. Photomicrographs.

Figure 1. Hole 462A, Core 44, Section 2, 82–87 cm; olivine microphenocryst, including spinel and liquid inclusion in glass layer of pillow basalt.

Figure 2. Hole 462A, Core 47, Section 2, 46–50 cm; spinel attached to olivine.

Figure 3. Hole 462A, Core 69, Section 2, 69–72 cm; clinopyroxene and plagioclase aggregates in glass layer of pillow basalt.

Figure 4. Hole 462A, Core 74, Section 4, 25–31 cm; subophitic texture in the center of a thick sill (crossed nicols).